This paper describes objective technical results and analysis. Any subjective views or opinions that might be expressed in the paper do not necessarily represent the views of the U.S. Department of Energy or the United States Government.

SAND2022-16622C

High Temperature Gladstone-Dale Coefficient Measurements in a Free-Piston Shock Tube

Gwendolyn T. Wang[1]
Georgia Institute of Technology, Atlanta, GA, 30332, USA

Kyle A. Daniel[2], Kyle P. Lynch[3], and Daniel R. Guildenbecher[4]
Sandia National Laboratories, Albuquerque, NM, 87185, USA

Yi Chen Mazumdar[5]
Georgia Institute of Technology, Atlanta, GA, 30332, USA

Accurately measuring aero-optical properties of non-equilibrium gases is critical for characterizing compressible flow dynamics and plasmas. At thermochemical non-equilibrium conditions, excited molecules begin to dissociate, causing optical distortion and non-constant Gladstone-Dale behavior. These regions typically occur behind a strong shock at high temperatures and pressures. Currently, no experimental data exists in the literature due to the small number of facilities capable of reaching such conditions and a lack of diagnostic techniques that can measure index of refraction across large, nearly-discrete gradients. In this work, a quadrature fringe imaging interferometer is applied at the Sandia free-piston high temperature shock tube for high temperature and pressure Gladstone-Dale measurements. This diagnostic resolves high-gradient density changes using a narrowband analog quadrature and broadband reference fringes. Initial simulations for target conditions show large deviations from constant Gladstone-Dale coefficient models and good matches with high temperature and pressure Gladstone-Dale models above 5000 K. Experimental results at *7653 K* and *7.87 bar* indicate that the index of refraction approaches high temperature and pressure theory, but significant flow bifurcation effects are noted in reflected shock.

I. Introduction

As research into hypersonic regimes, compressible flow fields, and plasmas grows, so does the need for experimental validation. In particular, reliable optical property measurements of high temperature gases are necessary to characterize optical aberrations through hypersonic boundary layers [1], in nonequilibrium plasma [2], and other complex phenomena. The ratio between the index of refraction and density, which is represented by the Gladstone-Dale (GD) relation, is a wavelength-specific constant at low to moderate temperatures (< 5000 K). However, as increased temperatures excite the internal degrees of freedom of molecules, their electric and optical properties change. The vibrational relaxation and dissociation of oxygen is known to significantly affect the GD of air [3]. To the authors' knowledge, no accurate experimental validation has been done at high pressures and temperatures due to difficulties in replicating and measuring high-enthalpy flows.

Since moderate to high pressure conditions are required to measure significant differences between constant and non-constant refractive index predictions, high enthalpy systems are needed to generate validation data. Facilities capable of reaching non-equilibrium conditions include expansion tunnels [4,5] and reflected shock systems [6,7].

[1] Ph.D. Student, Woodruff School of Mechanical Engineering. gtwang@gatech.edu.
[2] Member of Technical Staff, Aerosciences Department, AIAA Senior Member.
[3] Senior Member of Technical Staff, Aerosciences Department, AIAA Senior Member.
[4] Distinguished Member of Technical Staff, Engineering Sciences Center, AIAA Associate Fellow.
[5] Assistant Professor, Woodruff School of Mechanical Engineering, AIAA Senior Member, ellen.mazumdar@gatech.edu.

Sandia National Laboratories is a multimission laboratory managed and operated by National Technology & Engineering Solutions of Sandia, LLC, a wholly owned subsidiary of Honeywell International Inc., for the U.S. Department of Energy's National Nuclear Security Administration under contract DE-NA0003525.

Expansion tunnels are used for creating flight-conditions but result in a cold flow and low pressure due to the expansion. For the conditions of interest, a reflected shock tube is needed. Shock tube impulse devices rely on a high-pressure driver to burst a diaphragm, which initiates a shock wave in the test gas, raising the temperature and pressure. When the wave hits the endwall, a reflected shock propagates back, further increasing the thermodynamic state. Depending on the initial parameters, the incident or reflected shock can heat the test gas to target conditions where dissociation occurs. However, the test time behind the shock can be extremely short and large, nearly-discrete changes occur at the shock wave boundaries, which introduces further measurement challenges.

Therefore, in addition to having a capable experimental facility, a high resolution, ultra-speed diagnostic tailored for shock facility measurements is necessary. Few diagnostic techniques can resolve large index of refraction changes across a nearly-discrete boundary. Historic density-based measurements include two-dimensional (2D) fringe counting [8–10] and angled beam refraction [11]. Fringe counting has been used to determine dissociation characteristics of oxygen and nitrogen in the 1960s. Angled beam refraction has also been explored but requires specialized angled windows, tilted beams, or long beam paths. Due to difficulties in resolution and timing, previous fringe counting techniques have been low resolution and no experimental data in the literature exits beyond ~5000 K at high pressures. Fortunately, more recent developments in ultra-fast cameras with high resolution have greatly broadened the applications of laser diagnostics. To overcome past challenges, the authors developed a quadrature fringe imaging interferometer (QFII) to optically track large discrete changes of index of refraction at high resolution over tens or hundreds of fringes [12–14]. This method can be coupled with an ultra-high-speed camera to directly measure refractive index in dynamic environments.

In this work, we apply the QFII diagnostic to Sandia's free-piston high-temperature shock tube (HST) to experimentally measure the GD coefficient of air at high temperature and pressure conditions. Sandia's experimental facility uses a free piston to compress the driver gas, which allows it to reach more extreme conditions than other shock tubes[15]. Since reaching a high temperature at moderate pressures is difficult to obtain across the incident shock, the reflected shock condition is examined here. Use of this facility along with the QFII diagnostic reveals aero-optical properties of air above 5000 K at high pressures for the first time. In this paper, high temperature air properties simulated with the NASA CEA program are first shown to determine the expected GD deviation. Here, the refractivity changes due to differences in species concentration as molecules reach higher energy states, which is therefore dependent on temperature and pressure. After the simulations are outlined, the diagnostic capabilities and calibration process are discussed in further detail. Lastly, experimental data is presented with discussions on reflected shock flow features and comparisons to theory.

II. Non-equilibrium Simulations

Several simulations are shown here to identify regions where the GD coefficient deviates from a constant assumption for air. The composite GD for a gas mixture, K, is found with,

$$K = \frac{n-1}{\rho} = \sum K_i \frac{\rho_i}{\rho},$$

where n is the mixture index of refraction, i denotes each species, and ρ is the mixture density. Using a NASA CEA calculator in MATLAB, the refractivity dependence on temperature and pressure can be found using the species mole fractions. The GD coefficients for each gas species is a wavelength dependent property and are tabulated in Table 1 for a few wavelengths. Values for N_2, O_2, and NO are derived from [16] and values for atomic N and O are estimated from [8,17].

Table 1. Gladstone-Dale Coefficients of Gas Species

Species	λ = 405 nm [m^3/kg]	λ = 532 nm [m^3/kg]	λ = 633 nm [m^3/kg]
N_2	2.44e-4	2.40e-4	2.38e-4
O_2	1.95e-4	1.91e-4	1.89e-4
NO	2.27e-4	2.21e-4	2.19e-4
N	3.00e-4	3.10e-4	3.20e-4
O	1.98e-4	2.05e-4	1.81e-4

In Figure 1(a), the relation between Gladstone-Dale coefficient and temperature at a specific pressure (*P = 100 psi*) is shown. Slight deviations from the constant assumption begin to occur near 4000 K, when O_2 starts to dissociate. The refractivity continues to fluctuate more significantly as the N concentration also increases. In Figure 1(b), the pressure dependence of the composition GD can be seen clearly. A similar trend can be observed for all cases, but the deviation is most significant at low pressures and high temperatures. However, when designing target conditions from simulations, it is important to note that interferometry is a density-based measurement. Although the GD deviations are most prominent at low pressures, the density must be large in order to see an appreciable difference between the index of refraction with constant GD assumption and the non-linear calculation. High temperature conditions behind the incident shock are therefore less favorable since they generate lower pressures and result in small density changes, which lead to higher measurement uncertainties. Instead, post-reflected shock conditions at moderate pressures are considered in this work in order to obtain significant changes in the Gladstone-Dale coefficient and lower measurement uncertainties.

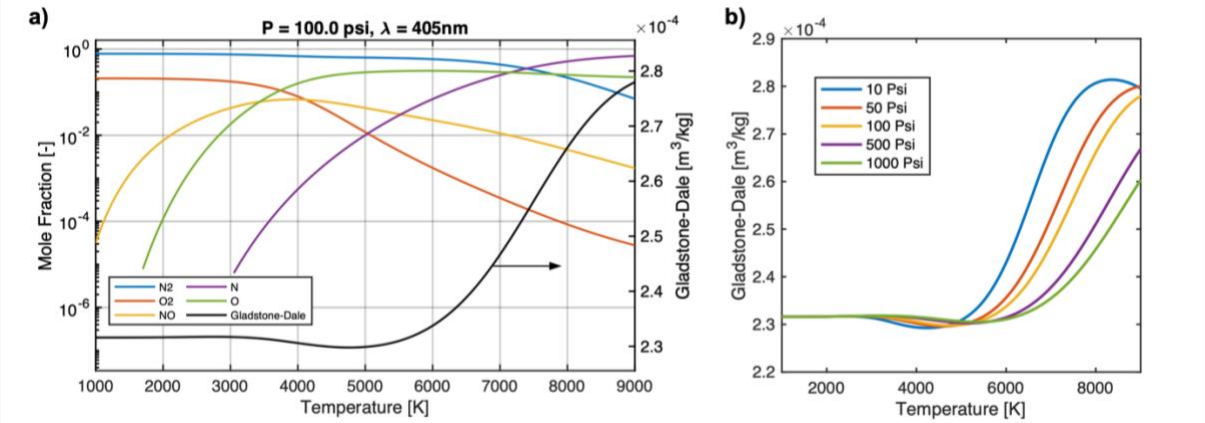

Figure 1. (a) The mole fractions for five species and the corresponding Gladstone-Dale coefficient are illustrated. (b) The composite Gladstone-Dale coefficient at various pressures is also shown.

III. Quadrature Fringe Imaging Interferometer

The QFII diagnostic is a Mach-Zehnder interferometer with two combined sources: a narrowband laser and a broadband light. By using two distinct sources, this technique implements a high-resolution quadrature while simultaneously tracking large index shifts with broadband fringes. The method is briefly described here and is shown in Figure 2, but further information can be found in previous work [14]. In this scheme, two sinusoidal signals are spatially selected from the narrowband electric field interference pattern to form an analog quadrature. The signals should be offset with a phase shift ($\pi/4$ is optimal) and are then fed into a quadrature equation to automatically track the change in index of refraction. Signals can be obtained from a calibration camera or from two photodetectors. In general, camera images allow for better flexibility in cases where the fringe spacing or the phase may change. Resolution in refractive index can be as high as 7×10^{-8} for a single-pass system depending on pixel noise and camera resolution [18].

While the narrowband signal is used to generate the quadrature, the broadband fringes are required to provide an absolute reference for large discrete changes. Sources with wide spectrum only produce interference patterns near the center of the interferometer. The pattern typically has a strong center with fringes decaying in intensity on either side. Since the finite fringes only appear over a small range, the QFII uses the center fringe as an absolute reference for large fringe movements. The measurement range may be extended by adding tilted glass delay plates. By dividing the beam into two or more columns using these glass plates, additional delays are set for each column, which greatly

increases the viewable dynamic range. At the imaging plane, the distinct fringe patterns for the narrowband and broadband columns are viewed side-by-side.

This optical system is calibrated by pumping the driven section down to vacuum. As the pressure drops, the narrowband quadrature records the change in index of refraction. Here, a reference ambient index of refraction is necessary, which can be determined by measuring the ambient pressure and temperature. Since calibration occurs near ambient conditions, the relation between refractivity and pressure is linear and can be easily validated. At the same time, the relative position of the center fringe in the broadband columns is obtained through a center tracking algorithm. The center locations are then mapped back to absolute index of refraction through the narrowband calculation. In this way, the absolute index of refraction can be obtained from a single image. Using the narrowband quadrature obtains the highest resolution. However, calibration can be difficult if there are facility or room vibrations, thus high resolutions cannot always be achieved. If noise levels are large, the calibration procedure can be modified so that the broadband pattern generates the index vs. pressure curve, and the narrowband is used to reduce uncertainty.

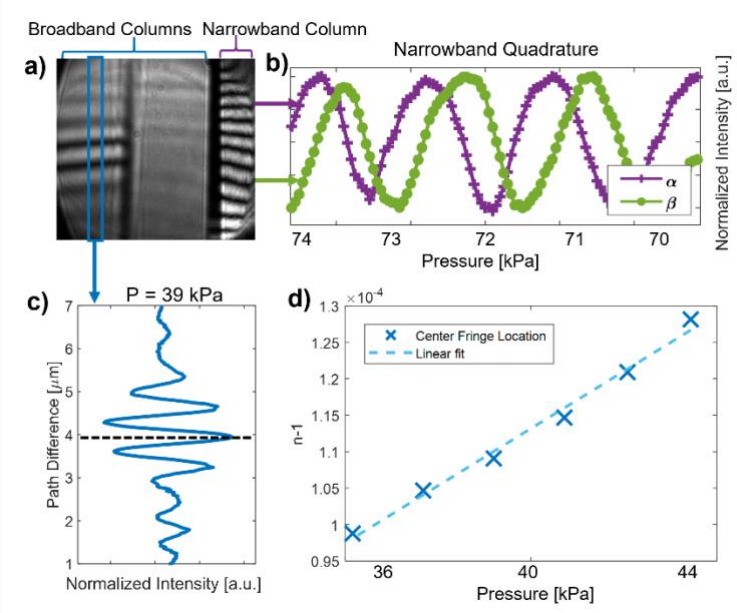

Figure 2. (a) The broadband fringe pattern is separated from the narrowband fringes using a short pass dichroic mirror on the right and a long pass filter on the left. (b) Two quadrature signals are spatially selected from the narrowband pattern for calibration. (c) After identifying the center fringe location on the broadband fringes, (d) the absolute index of refraction can be found using the quadrature calibration and a linear fit. This data comes from experiments conducted with the Georgia Tech shock tube facility [18].

IV. Experimental Setup

The free-piston facility at Sandia was developed and designed to achieve a wide range of high enthalpy conditions. To reach high temperatures and pressures, the tube relies on a 35 kg piston driven by a fill tank to compress the driver gas, as seen in Figure 3(a). The diaphragm bursts after compression and the shock wave propagates down the driven section, enabling it to reach conditions unobtainable by traditional shock tubes. Specific target conditions are reached by tuning the driver pressure and composition (typically He and Ar) as well as the piston reservoir pressure and the orifice plate diameter. The stainless-steel square test section and the end of the driven section has and inner width of 7.32 cm and 50.8 mm diameter sapphire windows which are 25 mm thick. Multiple PCB piezoelectronic pressure transducers are placed upstream to calculate wave speed and one is placed at the center of the endwall. Flow properties in the post-initial and post-reflected shock are determined with wave speed calculations and the NASA CEA code in MATLAB.

The QFII is placed at the test section as shown in Figure 3(b). The narrowband source is a 405 nm CW laser (Thorlabs CPS405) and the broadband source is a supercontinuum laser (SuperK EVO). The two sources are combined with a long-pass dichroic mirror and diverted through a 50/50 beam splitter. The experimental leg passes through two windows in the test section while the reference leg travels around the endwall. The location of the beam in the test section was approximately 1.5 cm away from the endwall and 3.5 cm above the bottom wall. Windows of identical thickness are used to match beam delay and divergence in the reference leg. Here, a micrometer stage balances and offsets the interferometer depending on the target conditions. In order to increase the range of viewable indices, a glass delay plate can be placed in each leg. After the beams are recombined, the sources are separated with a short-pass dichroic mirror and a colored glass filter to view the broadband and narrowband patterns simultaneously on a camera sensor. Images are taken with an ultra-high-speed (UHS) Shimadzu HPV-X2 camera, which is triggered off the endwall PCB.

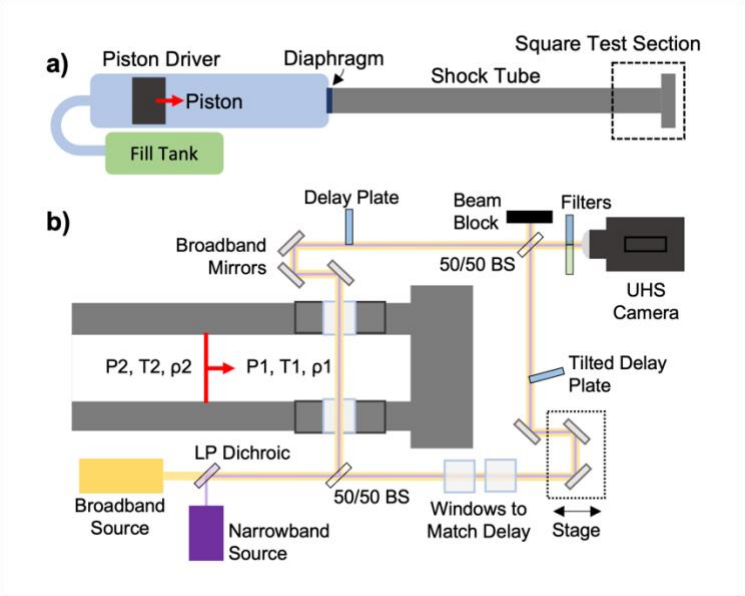

Figure 3. (a) The free-piston facility at Sandia consists of a piston driver, a shock tube, and the test section near the endwall. (b) The QFII system is arranged around the test section as shown.

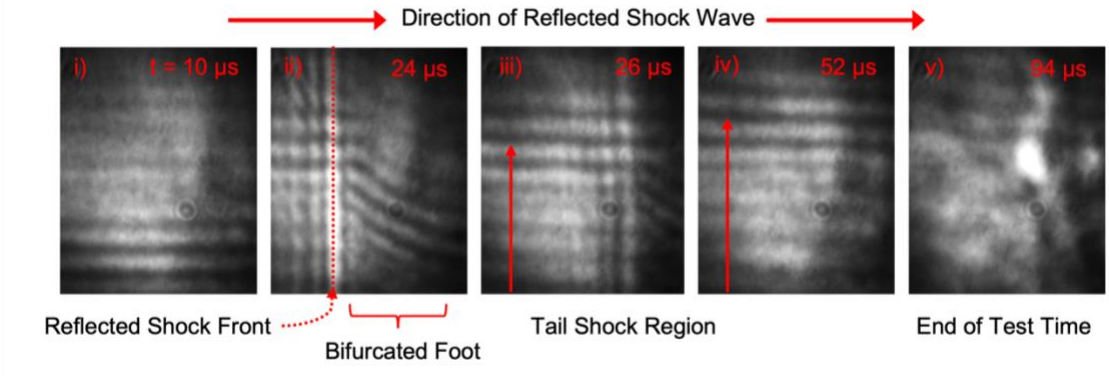

Figure 4. Images of the broadband interference is shown here (1 MHz frame rate, 200ns exposure). The reflected shock front moves from left to right.

V. Results and Discussion

The post-reflected shock conditions provide insight into the Gladstone-Dale relation as well as important flow characteristics. In the experiment shown in Figure 4, the driver gas is a mixture of He and Ar (85% He, 15% Ar) and the driven gas is dry air. The incident shock wave of $M_s = 13.95$ produces a post-reflected shock condition of $T_5 = 7653\ K$ and $P_5 = 7.87\ bar$. Here, the post-incident shock and post-reflected shock conditions, state 2 and state 5 respectively, were close to be viewable within the range of the QFII calibration. For experiments where this is possible, identifying the state 2 conditions further validates the state 5 measurements.

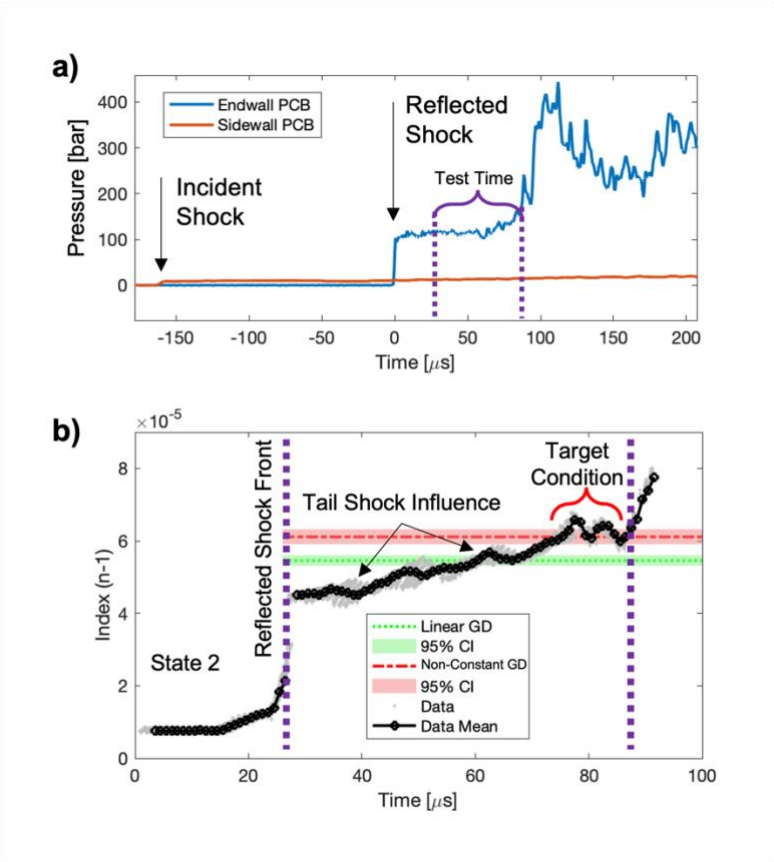

Figure 5. (a) The sidewall PCB is located 0.4 m upstream of the endwall. The dashed purple lines indicate the post-reflected shock test time. (b) The conditions for state 5 are $T_5 = 7653\ K$, $P_5 = 7.87\ Bar$, $\rho_5 = 0.24\ kg/m^3$. Error bars for the index measurements are $\pm\ 7.28e\text{-}7$ from the 95% CI during the calibration.

In general, post-incident shock conditions are very stable in shock tubes, but the reflected shock can generate complex flow bifurcation when the reflecting shock front interacts with boundary layers. In the interferogram images, the broadband fringe pattern clearly rises right before the reflected shock front, which corresponds to the bifurcated foot region. Here, broadband fringes moving upwards corresponds to an increasing index of refraction and 0 μs corresponds to the endwall PCB trigger. After the front passes, the fringe position gradually rises for 50 to 60 μs before increasing sharply. This is most likely caused by the tail shock region of the flow bifurcation behind the shock front, where the boundary layer interaction generates a lower enthalpy region. The time frame for the fluctuations of the index and the and the P_5 pressure indicates that this is caused by flow effects rather than thermodynamic non-equilibrium in the gases. Shortly after, the fringes quickly move out of the measurement range and turbulence dominates the image. These features are also observed in the corresponding pressure trace of the endwall and nearest sidewall PCB in Figure 5(a) as well as the calculated absolute index of refraction in Figure 5(b). The bifurcated foot is captured with the rise in index right before the reflected shock front. Across the front, a discrete change in index is seen, then the gradual rise as the tail shock passes. Around 75 μs, the index fluctuates around the calculated T_5, P_5 condition shortly before going out of frame. The sudden rise in index at the end of the test section may be explained

by the auto-ignition of air. Recombination reactions of N and O rapidly increases the pressure, which can be seen in the endwall pressure trace.

Uncertainty in the wave speed is calculated with a Monte Carlo statistical simulation based on the width of the PCBs. This 95% confidence interval is then propagated through the NASA CEA code to generate uncertainty in density. At $T_5 = 7653\ K$ and $P_5 = 7.87\ bar$, the non-linear index of refraction is significantly higher than the linear assumption. However, due to the bifurcation features, the measured index does not remain steady enough to conclude that it reached the non-linear GD. Several more experiments were carried out at similar conditions but due to variabilities in the bifurcation, the measured index of refraction did not reach a steady state at the expected conditions.

VI. Summary and Conclusion

Experimental measurements of the high temperature and pressure Gladstone-Dale relationship are currently nonexistent due to challenges in replicating and resolving high-enthalpy conditions. High temperatures and moderate to high pressures are necessary to produce density gradients large enough for a low-uncertainty interferometric diagnostic. By combining the experimental capabilities of the Sandia HST with the QFII diagnostic, index of refraction measurements are taken at conditions above 5000 K at high pressures for the first time. Results show that post-reflected shock conditions may appear to converge with the theory, but flow bifurcation and turbulence can greatly affect the measurements. In particular, post-reflected shock conditions may fail to reach a steady state before expansion waves further disrupt the flow. Therefore, further measurements are necessary to validate the non-linear optical properties of high-temperature air.

Acknowledgments

The authors would like to thank members of the Sensing Technologies Laboratory at Georgia Tech for their assistance with algorithm development and diagnostic setup. The authors would like to acknowledge the Sandia National Laboratories Academic Alliance Laboratory Directed Research and Development (LDRD) program for funding this research. Sandia National Laboratories is a multimission laboratory managed and operated by National Technology and Engineering Solutions of Sandia, LLC., a wholly owned subsidiary of Honeywell International, Inc., for the U.S. Department of Energy's National Nuclear Security Administration under contract DE-NA0003525. This paper describes objective technical results and analysis. Any subjective views or opinions that might be expressed in the paper do not necessarily represent the views of the U.S. Department of Energy or the United States Government.

References

[1] Mackey, L. E., Boyd, I. D., Leger, T., and Jewell, J. S. Turbulent Hypersonic Flow Effects on Optical Sensor Performance. Presented at the 2018 Fluid Dynamics Conference, 2018.

[2] Wu, Y., Tropina, A. A., Miles, R. B., and Limbach, C. M. "Measurements of N2 Refractive Index and Scalar Polarizability in a Pulsed Nanosecond Non-Equilibrium Discharge by Mach–Zehnder Interferometry and Spontaneous Raman Scattering." *Journal of Physics D: Applied Physics*, Vol. 53, No. 48, 2020, p. 485203.

[3] Lukhovitskii, B., Sharipov, A., Arsent'ev, I., Kuzmitskii, V., and Penyazkov, O. "On the Refractive Index of a Gas under High-Thermal-Nonequilibrium Conditions." *Journal of Engineering Physics and Thermophysics*, Vol. 93, No. 4, 2020, pp. 850–857.

[4] Dufrene, A., Sharma, M., and Austin, J. "Design and Characterization of a Hypervelocity Expansion Tube Facility." *Journal of Propulsion and Power*, Vol. 23, No. 6, 2007, pp. 1185–1193.

[5] MacLean, M., Dufrene, A., Wadhams, T., and Holden, M. Numerical and Experimental Characterization of High Enthalpy Flow in an Expansion Tunnel Facility. Presented at the 48th AIAA Aerospace Sciences Meeting Including the New Horizons Forum and Aerospace Exposition, 2010.

[6] Lynch, K. P., Grasser, T., Farias, P., Daniel, K., Spillers, R., Downing, C. R., and Wagner, J. L. Design and Characterization of the Sandia Free-Piston Reflected Shock Tunnel. Presented at the AIAA SciTech 2022 Forum, 2022.

[7] Nagamatsu, H. T., Geiger, R., and Sheer Jr, R. "Hypersonic Shock Tunnel." *ARS Journal*, Vol. 29, No. 5, 1959, pp. 332–340.

[8] Alpher, R. A., and White, D. R. “Optical Refractivity of High-Temperature Gases. I. Effects Resulting from Dissociation of Diatomic Gases.” *The Physics of Fluids*, Vol. 2, No. 2, 1959, pp. 153–161.
[9] Anderson, J. “Experimental Determination of the Gladstone-Dale Constants for Dissociating Oxygen.” *The Physics of Fluids*, Vol. 12, No. 5, 1969, p. I–57.
[10] Byron, S. “Shock-Tube Measurement of the Rate of Dissociation of Nitrogen.” *The Journal of Chemical Physics*, Vol. 44, No. 4, 1966, pp. 1378–1388.
[11] Kiefer, J., and Manson, A. “Refractive Index Change and Curvature in Shock Waves by Angled Beam Refraction.” *Review of Scientific Instruments*, Vol. 52, No. 9, 1981, pp. 1392–1396.
[12] Wang, G. T., and Mazumdar, Y. C. Quadrature Fringe Imaging Interferometer for Index of Refraction Measurements. Presented at the Laser Applications to Chemical, Security and Environmental Analysis, 2020.
[13] Wang, G., and Mazumdar, Y. C. High-Gradient Index of Refraction Measurements with a Quadrature Fringe Imaging Interferometer. Presented at the AIAA Scitech 2021 Forum, 2021.
[14] Wang, G., Peng, Y., Sun, W., and Mazumdar, Y. C. Shock Tube Index of Refraction Measurements Using a Quadrature Fringe Imaging Interferometer. Presented at the AIAA SciTech 2022 Forum, 2022.
[15] Lynch, K. P., and Wagner, J. L. A Free-Piston Driven Shock Tube for Generating Extreme Aerodynamic Environments. In *AIAA Scitech 2019 Forum*, American Institute of Aeronautics and Astronautics.
[16] Gardiner, W. C., Hidaka, Y., and Tanzawa, T. “Refractivity of Combustion Gases.” *Combustion and Flame*, Vol. 40, 1981, pp. 213–219.
[17] Wettlaufer, D. E. “Specific Refractivities of Atomic Nitrogen and Oxygen.” *Physics of Fluids*, Vol. 15, No. 11, 1972, p. 2065.
[18] Wang, G. T., Peng, Y., Guildenbecher, D. R., Lynch, K. P., Sun, W., and Mazumdar, Y. C. “Hybrid Interferometric Diagnostic for the Refractive Index Measurement across Nearly Discrete Shock Waves.” *Optics Letters*, Vol. 47, No. 16, 2022, pp. 4159–4162.